Analysis of molecular subtypes and prognostic signature of senescence-associated secretory phenotype in pancreatic cancer

Yuewen Kuang, Mingkun Jia, Yuming Zhu and Zhiyong Xiang

Hepatobiliary and Pancreatic Surgery, The Third Affiliated Hospital of Chongqing Medical University (Fangda Hospital), Chongqing, China

ABSTRACT

Background. Pancreatic cancer (PC) exhibits an extremely poor prognosis due to its high heterogeneity. The senescence-associated secretory phenotype (SASP), a distinct secretory profile displayed by senescent cells, has been increasingly studied. However, the role of SASP in PC prognosis and treatment remains unclear.

Methods. Transcriptomic sequencing data from PC patients were analyzed using consensus clustering based on SASP genes. A prognostic signature was subsequently constructed *via* Least Absolute Shrinkage and Selection Operator (LASSO) regression using survival-related SASP genes. Pathway enrichment analysis for distinct subgroups was performed using Gene Set Variation Analysis (GSVA). Comprehensive analyses of mutational landscapes and tumor immune microenvironments were conducted across risk-stratified PC samples.

Results. Consensus clustering based on SASP genes identified two SASP-associated clusters (SASPclusters), with cluster B demonstrating significantly worse prognosis than cluster A. Thirty-three SASP genes showed significant associations with PC prognosis, and a 7-gene SASP-based prognostic signature was established. High-risk patients exhibited significantly higher mutation rates. Distinct immune cell infiltration patterns, immune functions, checkpoint expression levels, and chemosensitivity profiles were observed between risk groups. Besides, we found that ANGPTL4 could promote PC cell proliferation, migration, and invasion.

Conclusion. Molecular subtyping and risk stratification based on SASP genes effectively predict PC prognosis and reveal heterogeneity in mutational burden, immune microenvironment, and therapeutic sensitivity. These computational findings deepen our understanding of potential role of SASP in PC and provide a theoretical foundation for personalized treatment strategies.

Subjects Bioinformatics, Computational Biology, Gastroenterology and Hepatology, Oncology, Data Mining and Machine Learning

Keywords Pancreatic cancer, Senescence-associated secretory phenotype, Tumor microenvironment

Submitted 5 June 2025
Accepted 4 November 2025
Published 6 January 2026

Corresponding author
Zhiyong Xiang,
18809892771@163.com

Academic editor
Nicole Nogoy

Additional Information and Declarations can be found on page 18

DOI **10.7717/peerj.20476**

Copyright
2026 Kuang et al.

Distributed under
Creative Commons CC-BY 4.0

OPEN ACCESS

INTRODUCTION

Pancreatic cancer (PC), predominantly pancreatic ductal adenocarcinoma (PDAC), is the most aggressive malignancy of the digestive system, with a five-year survival rate

(SR) of ∼12% (*Siegel et al., 2023*). The pancreas is anatomically concealed; hence, most PC patients are often diagnosed at advanced stages—a phenomenon that is projected to make PC the second deadliest malignancy by 2030 (*Nevala-Plagemann, Hidalgo & Garrido-Laguna, 2020*; *Park, Chawla & O'Reilly, 2021*; *Rahib et al., 2021*). While surgical resection remains the standard intervention for PC, adjuvant therapies, neoadjuvant treatments, immunotherapy, targeted therapy, and radiotherapy (RT) have demonstrated transient efficacy in select populations, although often followed by drug resistance (*Mizrahi et al., 2020*). Additionally, various factors, including cellular senescence—an emerging focus in cancer research—modulate the tumor microenvironment (TME), highlighting its complex nature, which confers limited response to cytotoxic therapies and immunotherapy in PC patients (*Park, Chawla & O'Reilly, 2021*).

Cellular senescence is a stress-triggered, irreversible proliferative arrest featuring structural and functional degeneration (*Dong et al., 2024*; *McHugh, Durán & Gil, 2025*). Senescence, which was initially recognized as replicative senescence in human fibroblasts, presently encompasses oncogene-induced, therapy-induced, virus-induced, mitochondrial dysfunction-associated, and immune-mediated forms (*Wang et al., 2024*). Besides growth arrest, senescent cells also exhibit Senescence-Associated Secretory Phenotype (SASP) (*Wang et al., 2024*), a hyper-secretory profile featuring the secretion of diverse proteins, cytokines, proteases, and chemokines (*Dong et al., 2024*). According to reports, SASP performs dual roles in tumorigenesis. In addition to inducing cell cycle arrest and immune-mediated damaged cell clearance to suppress tumor initiation, it also fosters immunosuppressive microenvironments conducive to tumor progression and metastasis (*Dong et al., 2024*; *Eggert et al., 2016*; *Liu & Hornsby, 2007*; *Orjalo et al., 2009*). Furthermore, SASP exerts context-dependent effects in PC. For instance, MEK and CDK4/6 inhibition-induced senescence promoted T-cell infiltration and tumor suppression in murine models (*Ohuchida et al., 2004*; *Ruscetti et al., 2020*), whereas radiation-induced fibroblast SASP enhanced PC invasiveness (*Ohuchida et al., 2004*). Nonetheless, the prognostic implications of specific SASP components in PC remain unclear, necessitating bioinformatics-driven identification of SASP-related prognostic biomarkers.

Herein, we stratified PC patients from the TCGA-ICGC cohort into two SASP subtypes based on the consensus cluster analysis results and established a 7-gene SASP-based prognostic signature. We also conducted functional experiments, validating the role of ANGPTL4 in promoting PC proliferation and metastasis. Our proposed risk stratification model could provide computational evidence to guide prognostic prediction and personalized therapy in PC.

MATERIALS & METHODS

Data collection

Transcriptomic sequencing and survival data for PC patients were obtained from The Cancer Genome Atlas (TCGA; https://portal.gdc.cancer.gov/) and the International Cancer Genome Consortium (ICGC) (PACA-AU cohort; https://dcc.icgc.org/), with gene expression matrices merged into the combined TCGA-ICGC dataset using the "ComBat"

function for batch correction. On the other hand, SASP gene sets were derived from previous literature (*Saul et al., 2022*), while Copy Number Variation (CNV) files for PC patients were downloaded from UCSC Xena (https://xenabrowser.net/). Additionally, a single-cell RNA sequencing dataset (GSE154778) comprising 10 primary and 6 liver metastatic samples was retrieved from the Gene Expression Omnibus (GEO) database.

Consensus clustering analysis

We performed consensus clustering utilizing the "ConsensusClusterPlus" R package to explore associations between SASP gene expression and PC subtypes. Survival differences between SASPclusters were compared using Kaplan–Meier (K-M) survival analysis. Gene Set Variation Analysis (GSVA) was performed using all genes from the TCGA-ICGC cohort before comparing differentially enriched pathways between the two SASPclusters and visualizing the results with a heatmap. Differentially Expressed Genes (DEGs) between clusters were identified using the "limma" package (log2FC >1, adjusted $p < 0.05$), followed by functional enrichment analysis.

Prognostic signature construction and validation

The prognostic value of SASP genes was assessed using Univariate Cox regression, and the prognostic signature was constructed using the Least Absolute Shrinkage and Selection Operator (LASSO) Cox regression. The combined TCGA-ICGC dataset was randomly partitioned into training and validation cohorts (1:1; 1,000 iterations) using the "caret" package. The optimal λ value was identified using LASSO regression with 10-fold cross-validation. Genes with non-zero coefficients at the optimal λ were selected, from which a 7-gene prognostic signature was constructed, and patients were stratified into low- and high-risk groups. Model performance was evaluated using receiver operating characteristic (ROC) curves generated using the "timeROC" package. Signature gene expressions were visualized using Heatmaps ("pheatmap"), and risk group separation was depicted with the principal component analysis (PCA).

Clinical relevance of the prognostic signature

Risk score correlations with clinicopathological features (age, sex, pathological grade, tumor nodes metastasis (TNM) stage, and SASPcluster) were analyzed. A nomogram ("rms") was then developed to predict PC patient survival. Drug sensitivity differences between risk groups were assessed using the "oncoPredict" package, while pathway enrichments across subtypes and risk groups were compared using "GSVA".

Mutation analysis

Tumor mutational burden (TMB) was calculated for each patient, with TMB-risk score associations established using Spearman correlation. The risk groups were compared for mutation frequency differences using "maftools".

Tumor immune infiltration analysis

Immune cell infiltration levels were quantified using the CIBERSORT algorithm. Immune cell distribution differences between risk groups were visualized using Violin plots. Associations between risk scores and immune cell infiltration were assessed using Spearman

correlation analysis with the ''psych'' package. Immune function activity and checkpoint expression disparities were evaluated using GSVA.

Single-cell RNA-seq analysis

Single-cell data underwent stringent quality control processes: nFeature_RNA >300 & <6,000, percent.mt <10, percent. HB <1, and nCount_RNA <50,000. Data normalization, variable gene identification (2,000 genes), scaling, and integration were performed using ''Seurat'' and ''harmony''. Dimensionality reduction was visualized using PCA and UMAP. Cell clusters (resolution = 2) were annotated based on marker genes.

Cell lines

Signature gene protein expression in normal and tumor tissues was validated using the Human Protein Atlas (HPA) (*Thul et al., 2017*). The MIA PaCa-2 and PANC-1 cell lines (Wuhan Pricella Biotechnology Co., Ltd., Wuhan, China) were cultivated in DMEM culture medium supplemented with 10% Fetal Bovine Serum (FBS; Gibco, Billings, MT, USA) and identified using Short Tandem Repeat (STR).

Cellular senescence induction

First, H_2O_2 was added to the cell culture medium to a final concentration of 50 mM and incubated at 37 °C for 2 h (*Purcell, Kruger & Tainsky, 2014*). Senescence was then detected using Western Blot (WB) analysis. The primary antibodies included anti-p21 antibody (10355-1-AP, 1:2000; Proteintech, Rosemont, IL, USA), anti-16 antibody (10883-1-AP, 1:3000; Proteintech, Rosemont, IL, USA), and anti-GAPDH antibody (60004-1-lg 1:50000; Proteintech, Rosemont, IL, USA).

Enzyme-Linked Immunosorbent Assay

Cell culture supernatants (CM) from H_2O_2-induced senescent PC and control cells were collected, and secreted protein levels of ANGPTL4 were measured using the ElaBoXTM Human Angiopoietin-like 4 Enzyme-Linked Immunosorbent Assay (ELISA) Kit (SEKH-0091; Solarbio, Beijing, China), with concentrations determined following the manufacturer's instructions.

Cell proliferation assay

Cell proliferation was assessed using the Cell Counting Kit 8 (CCK-8) kit (Beyotime Biotechnology, Shanghai, China). The cells (1,000/well) were seeded into 96-well plates and cultured with a recombinant ANGPTL4 protein. Absorbance (Optical Density (OD) 450 nm) was measured daily for 4 days.

Migration and invasion assays

Migratory and invasive capacities were evaluated using Wound healing and Transwell assays. For the wound healing assay, confluent cells in 6-well plates were scratched with a 200-μl pipette tip and cultured in serum-free medium containing rANGPTL4 (100 ng/ml). For the Transwell assay, cells in serum-free medium (5×10^4) were seeded into Matrigel-coated chambers (Corning, Corning, NY, USA), while complete medium containing rANGPTL4 (100 ng/ml) was added to the lower chamber and incubated for 48 h. Migrated cells were fixed (4% Paraformaldehyde (PFA)) and stained (crystal violet).

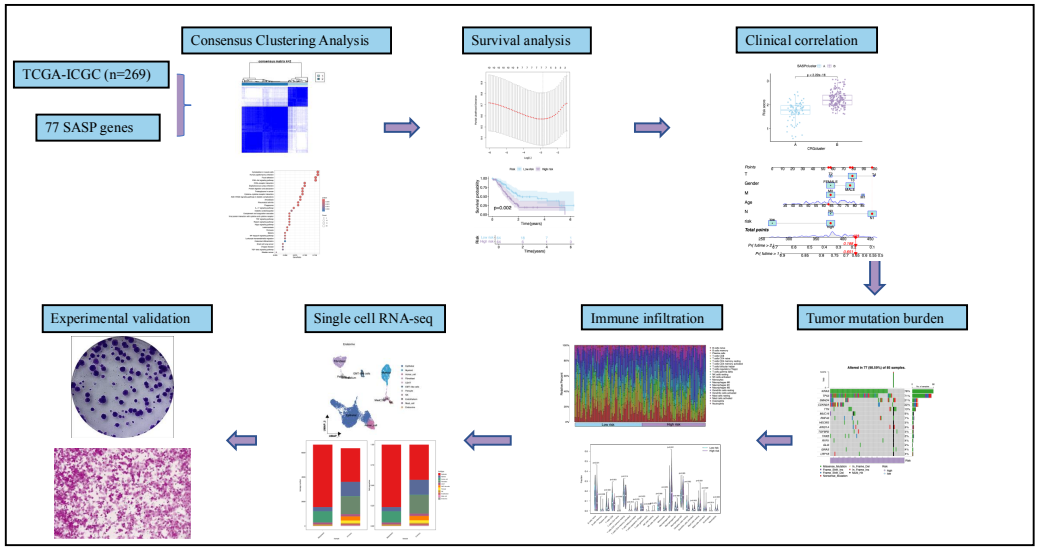


Figure 1 **Workflow.**

Full-size DOI: 10.7717/peerj.20476/fig-1

Statistical analysis

Analyses were conducted in R (v4.2.1). Random sampling ("caret") divided cohorts. Log-rank tests compared Kaplan–Meier survival curves. Spearman correlations assessed associations. Statistical significance thresholds: $^{***}p < 0.001$; $^{**}p < 0.01$; $^{*}p < 0.05$; ns $p > 0.05$.

RESULTS

Genetic alterations of SASP genes

Figure 1 summarizes the workflow, and Table S1 lists the 77 SASP genes. The merged TCGA-ICGC dataset comprised a cohort of 269 PC patients. Somatic CNV analysis revealed frequent alterations: CCL5, CCL7, and CCL2 exhibited copy number gains, while BMP6, VEGFC, and EDN1 showed losses (Fig. 2A).

Identification of SASP subtypes

The patients were stratified into two SASPclusters (A and B) using consensus clustering (Figs. 2B, 2C), with PCA confirming distinct separations (Fig. 2D). Compared to Cluster A, Cluster B exhibited significantly worse Overall Survival (OS) (Fig. 2E). Heatmaps further revealed elevated SASP gene expression in Cluster B (Fig. 2F), with GSVA also showing the enrichment of the glycolysis, Epithelial-Mesenchymal Transition (EMT), hypoxia, and PI3K-AKT-mTOR pathways in Cluster B (Fig. 2G). A consistent pattern of enrichment was observed in the Gene Set Enrichment Analysis (GSEA, Fig. 2H). Cluster comparisons identified 381 DEGs (Fig. 2I). Gene Ontology (GO) enrichment analysis revealed significant associations with Extracellular Matrix (ECM) organization and integrin binding (Fig. 2J). On the other hand, Kyoto Encyclopedia of Genes and Genomes (KEGG) pathway analysis

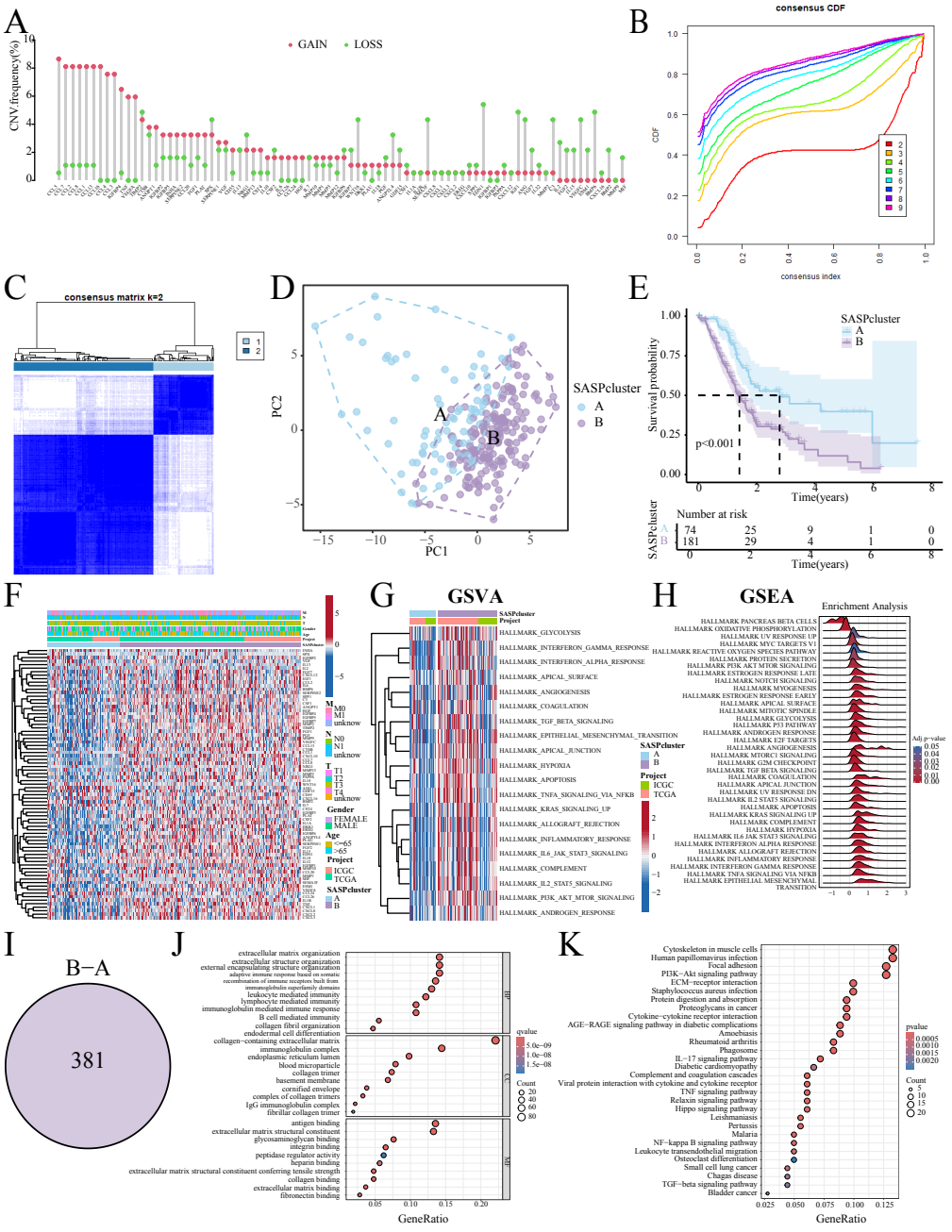


Figure 2 **SASP cluster identification.** (A) Bar graph showing the CNV frequency of SASP genes; (B, C) Consensus clustering analysis; (D) Sample distribution PCA plot for SASPclusters; (E) Survival plot for SASPclusters; (F) Heatmap depiction of SASP gene expression between SASPclusters; (G, H) GSVA and GSEA results of enrichment pathways between SASPclusters; (I) Venn plot of DEGs between SASPclusters; and (J, K). GO and KEGG bubble plots of DEGs between SASPclusters.

Full-size DOI: 10.7717/peerj.20476/fig-2

revealed enrichment in the ECM–receptor interaction, PI3K–Akt signaling, and cytokine–cytokine receptor interaction pathways (Fig. 2K).

Prognostic signature construction and validation

Univariate Cox regression identified 33 prognostic SASP genes (Fig. 3A), of which FGF1 (HR = 0.813), IGFBP2 (HR = 0.862), and VGF (HR = 0.865) emerged as protective factors. Protein-Protein Interaction (PPI) networks highlighted gene connectivity (Fig. 3B), with LASSO regression yielding a 7-gene signature: Risk score = (0.0081 × ANGPTL4) + (0.0086 × DKK1) + (0.0177 × EREG) + (0.0425 × IGFBP3) + (0.1902 × IL18) + (0.1702 × MMP13) + (0.0567 × PLAU) (Range: 0.58–3.22, Fig. 3C). Furthermore, high-risk patients exhibited shorter survival (Figs. 3D, 3E). High-risk patients also exhibited signature gene upregulation (Fig. 3F). The AUC values for the training cohort were 0.722 (1 year), 0.693 (2 years), and 0.677 (3 years); for the test cohort, they were 0.661 (1 year), 0.641 (2 years), and 0.626 (3 years). The overall cohort AUC values were 0.695 (1 year), 0.669 (2 years), and 0.644 (3 years). Compared to traditional clinical characteristics, the risk score demonstrated superior predictive performance in forecasting prognosis for patients with PC (Fig. 3G). The PCA plot demonstrates a clear separation between the two risk groups of patients (Fig. 3H).

Validation of signature genes in single-cell RNA-seq data

Quality control processes yielded 23 cell clusters (Figs. 4A, 4B). Furthermore, annotation revealed 11 cell types, with elevated ductal epithelial cells and fibroblasts in metastatic samples and primary tumors, respectively (Figs. 4C–4E). The signature genes were predominantly expressed in ductal epithelial and myeloid cells (Fig. 4F).

Clinical relevance of the prognostic signature

Higher risk scores correlated with advanced T-stage (Fig. 5A) and SASPcluster B (Fig. 5B), highlighting the significance of SASP in tumor development or risk. Furthermore, most SASP genes showed differential expression between groups (Fig. 5C). Multivariate Cox regression confirmed risk score as an independent prognostic factor (Figs. 5D, 5E), and GSVA and GSEA highlighted the enrichment of the glycolysis, mTORC1, and EMT pathways in high-risk patients (Figs. 5F, 5G). Moreover, the resulting nomogram effectively predicted survival (Figs. 5H, 5I).

Tumor mutational landscape

Low-TMB patients, particularly in the low-risk subgroup, exhibited better survival (Figs. 5J, 5K), and TMB correlated positively with risk scores (Fig. 5L). Furthermore, KRAS/TP53 mutations correlated with higher risk scores (Fig. 5M), and high-risk patients demonstrated greater mutation frequencies (90.59% *vs.* 70.42%; Fig. 5N).

Association of prognostic signature with TME

According to CIBERSORT analysis, high-risk patients exhibited naive B cell, memory B cell, plasma cell, and CD8+ T cell downregulation, alongside M0 macrophage and activated Dendritic Cell (DC) upregulation (Figs. 6A, 6B). The risk score exhibited a negative correlation with naïve B cells, plasma cells, and CD8 T cells, whereas it showed a positive correlation with Macrophage M0, Macrophage M2, and activated dendritic cells (Fig. 6C). Furthermore, in high-risk patients, immune functions (*e.g.*, Type I IFN response,

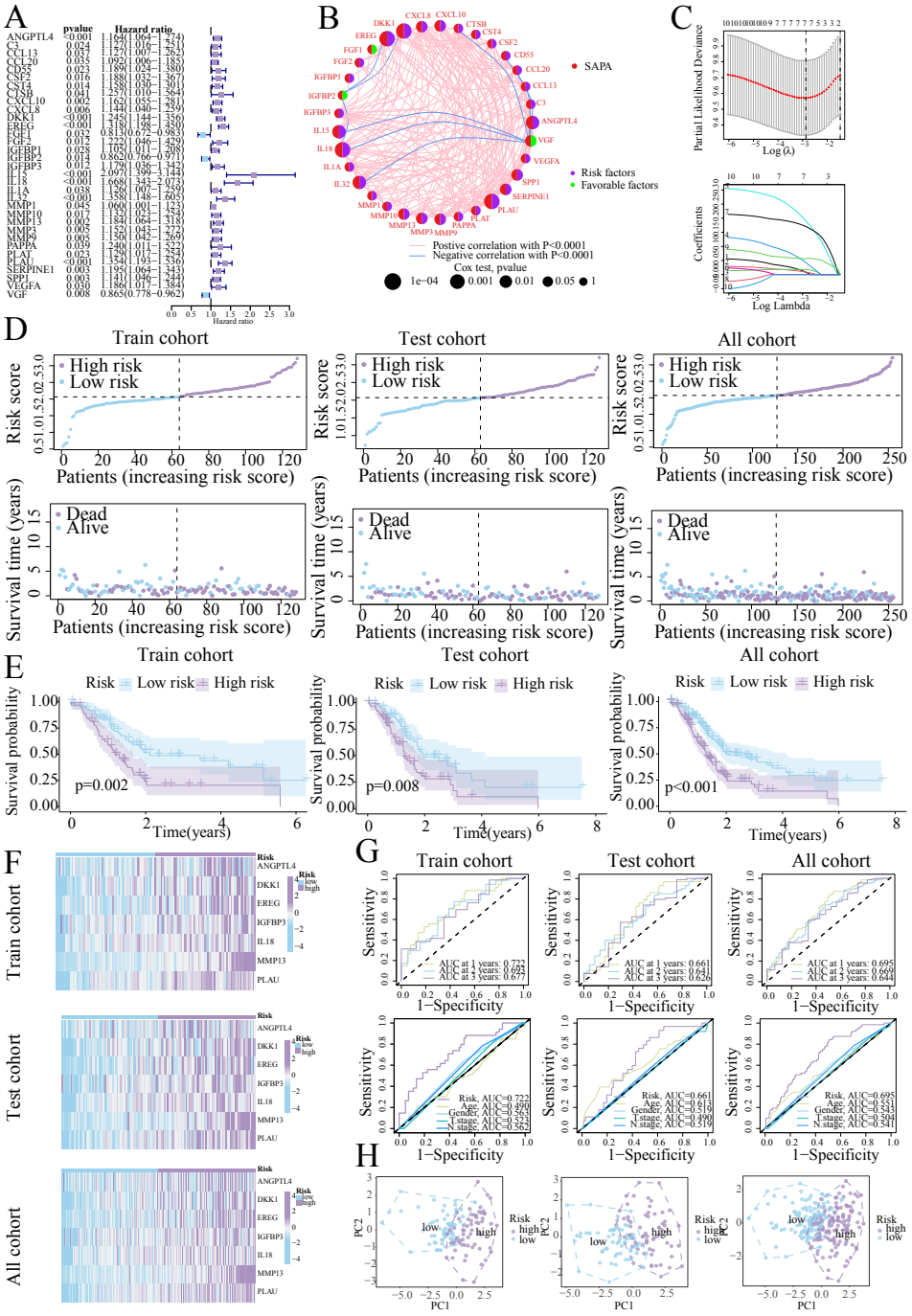


Figure 3 **Prognostic signature construction.** (A) Univariate Cox regression analysis of the SASP gene. (B) Interaction circle diagram of SASP genes. (C) LASSO regression to construct prognostic models. (D) Distribution of patients at different risks. (E) Survival curves for patients at different risks. (F) Heatmap of signature gene expression in patients with different risks. (G) ROC curves for patients at different risks. (H) PCA distribution of patients with different risks.

Full-size DOI: 10.7717/peerj.20476/fig-3

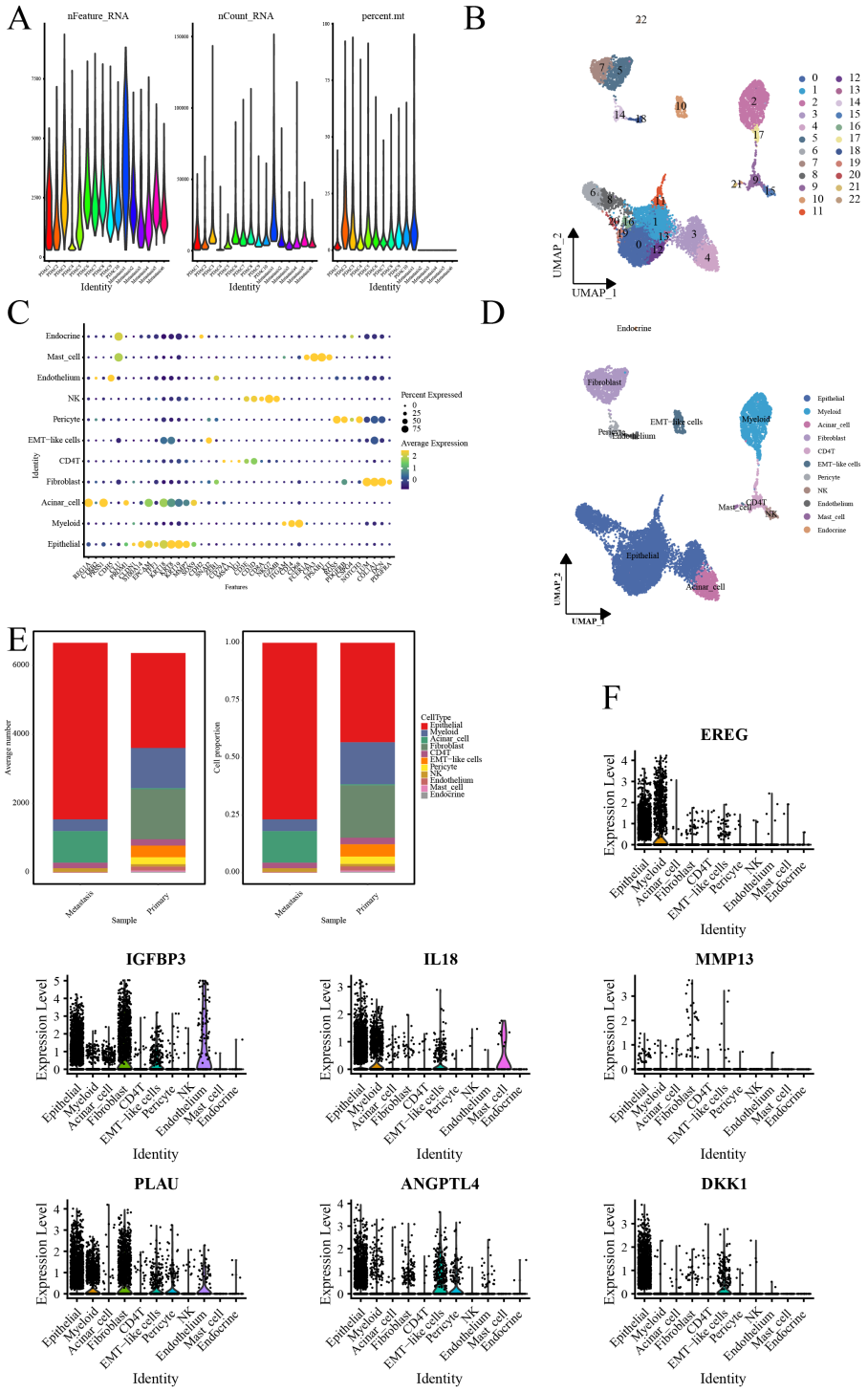


Figure 4 **Single-cell RNA-seq data analysis.** (A) Violin representation of each sample's data characteristics; (B) UMPA plots for cell clustering; (C) Bubble plot of cell marker genes for each cell type; (D) UMPA plots for cell types; (E) Bar graph showing the proportion of each cell type; and (F) Violin representation of the expression level of the signature genes in each cell.

Full-size DOI: 10.7717/peerj.20476/fig-4

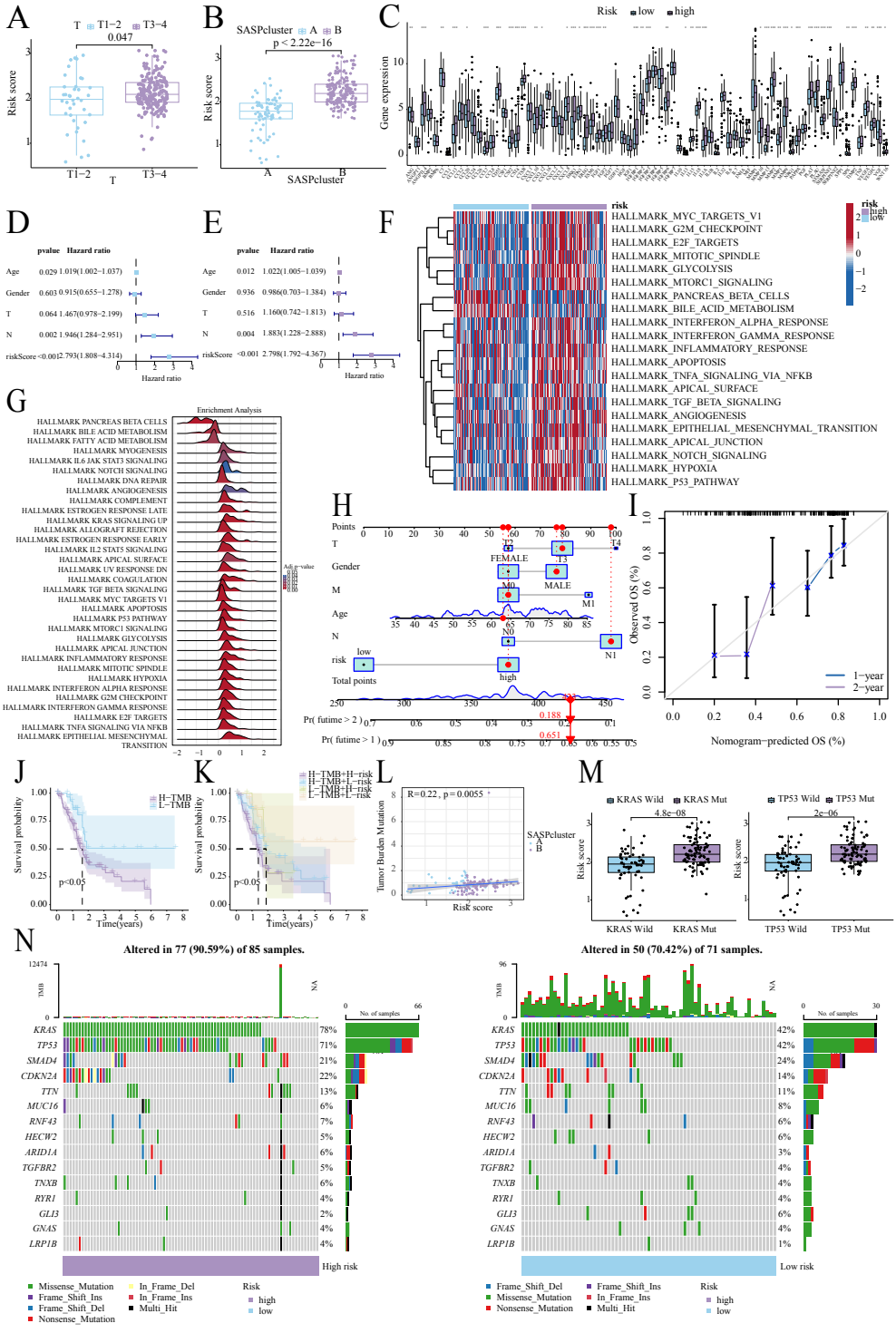


Figure 5 **Risk score-clinical characteristics relationship.** (A) Relationship between risk score and T stage; (B) Relationship between risk score and SASPcluster; (C) SASP gene expression across patients with different risk levels; (D, E). Univariate and multivariate Cox regression analysis; (F, G) GSVA and GSEA (continued on next page…)

Full-size DOI: 10.7717/peerj.20476/fig-5

Figure 5 (…continued)
results showing pathway enrichment between patients with different risk levels; (H, I). Nomogram construction and validation; (J, K). Survival curves for TMB and risk score; (L) Scatterplot of TMB and SASP-cluster correlations; (M) Scatterplot of risk score with KRAS and TP53 mutation frequency; and (N) Waterfall plot of risk score with gene mutations in PDAC samples.

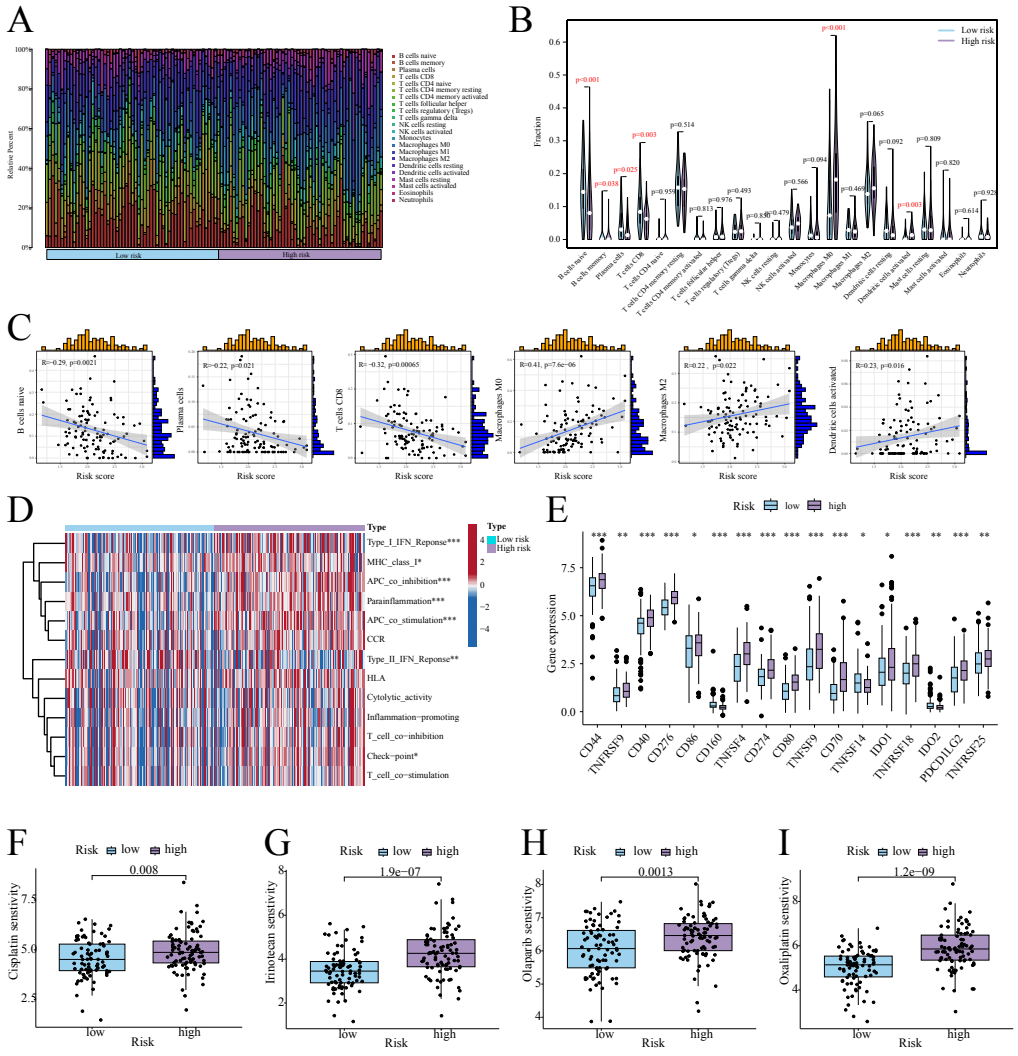


Figure 6 **Immune infiltration analysis.** (A) Histogram of the level of immune cell infiltration. (B) Violin plot of the level of immune cell infiltration. (C) Scatterplot of the correlation between the level of immune cell infiltration and risk score. (D) GSVA heatmap of immune function in patients at different risks. (E) Violin plots of immune checkpoint expression in patients at different risks. (F–I) Sensitivity to commonly used chemotherapeutic agents in patients at different risks. * indicates $p < 0.05$, ** indicates $p < 0.01$, *** indicates $p < 0.001$.

Full-size DOI: 10.7717/peerj.20476/fig-6

checkpoint activity) were suppressed (Fig. 6D), whereas checkpoints CD44, PD-L1, and PDCD1LG2 were upregulated (Fig. 6E). On the other hand, low-risk patients showed enhanced sensitivity to cisplatin, irinotecan, olaparib, and oxaliplatin (Figs. 6F–6I).

Functional validation of ANGPTL4 in PC

Centrosome amplification-induced senescence-associated secretory phenotype variation activated the Hypoxia-Inducible Factor-1α (HIF-1α) and related gene pathways, including migration-promoting factors such as ANGPTL4, highlighting the significance of ANGPTL4 in SASP (*Wu et al., 2023*). Herein, immunohistochemistry (IHC) analysis revealed ANGPTL4, IL-18, MMP13, and PLAU upregulation in PC tissues (Figs. 7A–7D). Furthermore, pan-cancer analysis revealed ANGPTL4 overexpression in PC, as well as breast, colorectal, and liver cancers (Fig. 7E). High ANGPTL4 expression correlated with a poor prognosis, poor differentiation, and lymph node metastasis (LNM) (Figs. 7F–7J). Additionally, GeneMANIA identified the interactions of ANGPTL4 with LPL, PPARD, and PPARG (Fig. 7K), with ANGPTL4 expression correlating positively with M0 macrophages, and negatively with NK cells activated and T cells CD4+ memory resting (Fig. 7L). We also detected the cellular senescence markers p21 and p16 to validate the construction of the oxidative stress (OS)-induced cellular senescence model (Fig. 8A). According to the ELISA results, senescent cells secreted significantly higher levels of ANGPTL4 compared to the control group, confirming ANGPTL4's involvement in SASP (Fig. 8B). Functional assays further demonstrated rANGPTL4-driven cell proliferation (Fig. 8C), migration, and invasion (Fig. 8D).

DISCUSSION

The global annual PC diagnosis has doubled over the past two decades, posing substantial challenges to public health systems and society as a whole (*Klein, 2021*). Furthermore, effective treatments for PC remain limited. Although immunotherapy and targeted therapies demonstrated great promise, the poor response attributed to the unique immunosuppressive TME of PC has introduced new challenges.

Cellular senescence, a biological concept first proposed in 1961, has extended beyond replicative exhaustion to include stress-induced senescence (*Dong et al., 2024*). Tumor heterogeneity dictates that senescence adopts the ''double-edged sword'' adage in cancer progression. While senescence restricts uncontrolled proliferation *via* cell cycle arrest or immune cell recruitment, SASP secretes factors that shape an immunosuppressive TME, thus promoting tumor progression (*Dong et al., 2024*; *McHugh, Durán & Gil, 2025*). Despite extensive research on senescence and SASP, their roles in PC remain unclear, forming the basis of this study, which aimed to explore the associations of SASP-related genes with PC molecular subtypes, prognosis, genetic mutations, TME infiltration, and chemosensitivity.

Our findings revealed two SASP-associated clusters (SASPclusters) based on SASP gene expression. Compared to Cluster A, Cluster B exhibited worse prognosis and higher SASP gene expression. Furthermore, a 7-gene prognostic model was constructed using LASSO regression, effectively stratifying the patients into high- and low-risk groups. High-risk patients exhibited signature gene overexpression, predominantly localized to epithelial and myeloid cells in single-cell RNA-seq analyses. Additionally, cancer-associated pathways, including glycolysis, angiogenesis, and EMT, were enriched in Cluster

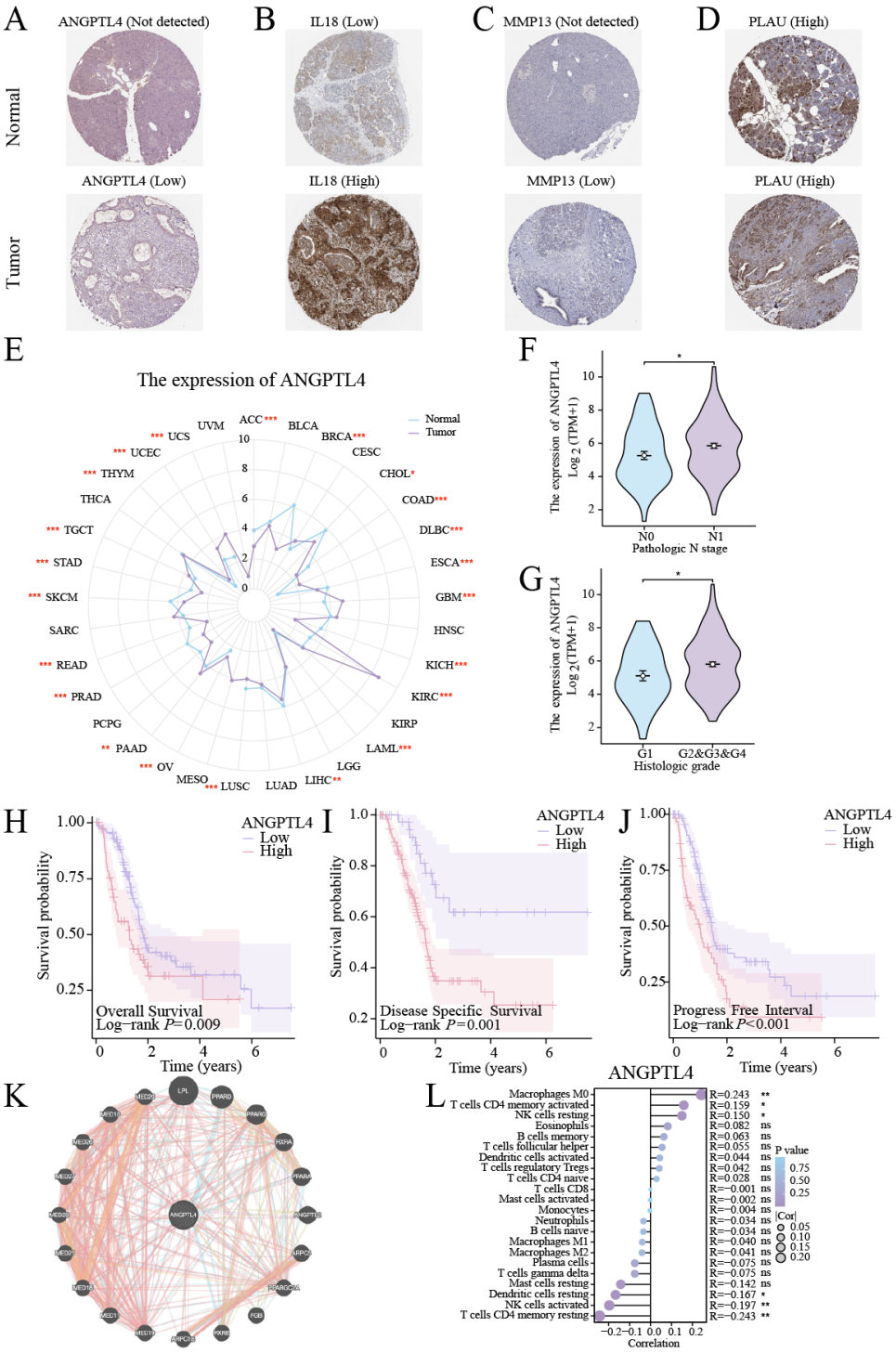


Figure 7 Analysis of ANGPTL4: (A–D) IHC image of the signature gene in the HPA database. (E) Radar plot of ANGPTL4 expression levels in pan-cancer. (F, G) Relationship between ANGPTL4 with tumor differentiation and PC lymph node metastasis. (H–J) Survival curves of ANGPTL4 in PC

(continued on next page…)

Full-size DOI: 10.7717/peerj.20476/fig-7

Figure 7 (…continued)
tissues. (K) Circle diagram of genes interacting with ANGPTL4. (L) Correlation of ANGPTL4 expression with the level of PC tissue immune cell infiltration. * indicates $p < 0.05$, ** indicates $p < 0.01$, *** indicates $p < 0.001$.

B and high-risk patients. *Nacarelli et al. (2019)* reported that the HMGA-NAMPT-NAD+ axis could enhance glycolysis and mitochondrial respiration, driving pro-inflammatory SASP. Furthermore, in preclinical PDAC models, therapy-induced senescence promoted angiogenesis *via* SASP-secreted factors, improving gemcitabine efficacy (*Ruscetti et al., 2020*). Similarly, senescent fibroblast-secreted SASP promoted EMT in premalignant epithelia (*Yang et al., 2018*), while myofibroblast-derived SASP facilitated EMT in oral submucous fibrosis (OSF) (*Sharma et al., 2021*), implying shared mechanisms between Cluster B and high-risk patients.

Chemotherapy and radiotherapy (RT) eliminate cancer cells, while making them, along with normal cells, senescent. Although cellular senescence could inhibit tumor progression, residual senescent cells post-treatment may pose new risks, such as promoting cancer stem cell (CSC) activation and re-proliferation, ultimately causing tumor recurrence (*Nardella et al., 2011*; *Milanovic et al., 2018*). Besides alleviating treatment-related side effects, combining senescent cell clearance with existing cancer therapies might also significantly reduce the risk of tumor progression (*Xiao et al., 2023*). Navitoclax (ABT263) could inhibit the activity of anti-apoptotic proteins, clearing senescent cells. It could also effectively eliminate PARP inhibitor olaparib-induced senescent ovarian and breast cancer cells (*Fleury et al., 2019*). Notably, navitoclax-galactose (Nav-Gal) could be a potent senescent cell clearance intervention, selectively inducing senescent cell apoptosis, with a senescent cell clearance index higher than that of navitoclax alone. It enhanced the cytotoxic effect of cisplatin in A549 lung cancer (LC) cells. Additionally, Cisplatin+Nav-Gal effectively eliminated senescent LC cells and significantly inhibited tumor growth (*González-Gualda et al., 2020*). Furthermore, artemisinin could inhibit irinotecan treatment-activated mTOR activity, alleviating irinotecan treatment-induced intestinal senescence. Moreover, drug combinations significantly inhibited colorectal tumor growth in mice (*Jia et al., 2023*). A combination formulation comprising ch282-5 and chloroquine, rapamycin, oxaliplatin, or navitoclax effectively inhibited colon cancer growth and liver metastasis (*Wang et al., 2016*). Overall, in addition to effectively inhibiting tumor progression, the combined use of chemotherapy drugs and the senescence-inducing agent navitoclax may improve high-risk patients' low sensitivity to drugs such as olaparib, cisplatin, irinotecan, and oxaliplatin, providing novel insights for clinical treatment.

Herein, the established model comprised several signature genes: IL18, MMP13, PLAU, IGFBP3, EREG, DKK1, and ANGPTL4. Interleukin-18 (IL-18) could downregulate the anti-aging protein Klotho, promoting fibroblast senescence in pulmonary fibrosis (*Zhang et al., 2019a*). In tumors, IL-18/IL-12-stimulated $\gamma\delta$ T cells directly kill cancer cells and induce senescence in the absence of TCR signaling, exerting potent anti-tumor activity (*Schilbach et al., 2020*). However, IL-18 is also recognized as a tumor-promoting factor (*Zhang et al., 2024*). This duality mirrors SASP's context-dependent roles, where IL-18

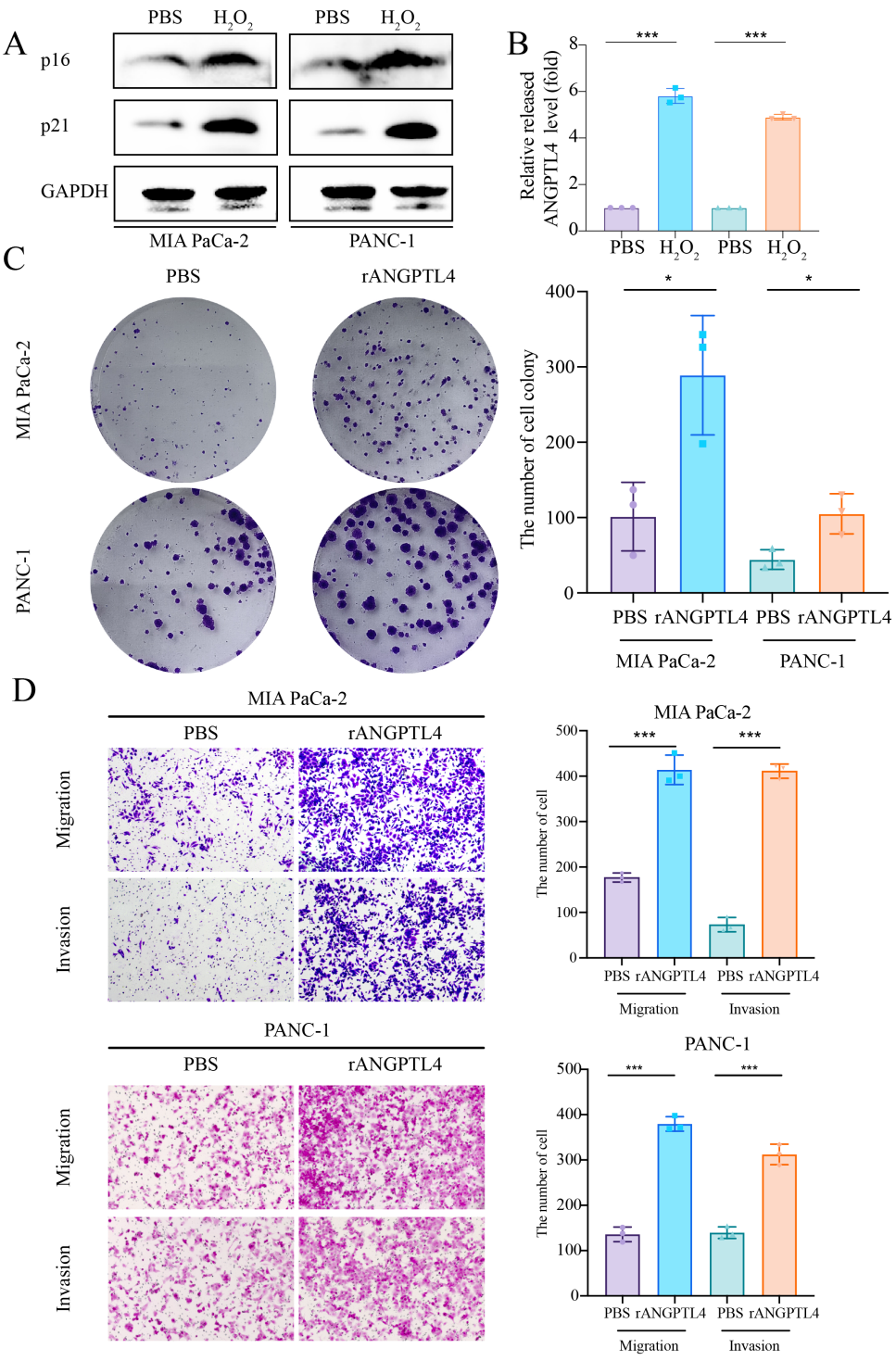


Figure 8 **Role of ANGPTL4 on PC proliferation and migration.** (A) Western blot detection of p21 and p16 to validate the cell senescence model. (B) ELISA for detecting ANGPTL4 levels secreted by senescent cells. (C) Clone formation results of rANGPTL4 promoting PC cell proliferation. (D) Transwell results of rANGPTL4 promoting PC cell migration and invasion (20x). * indicates $p < 0.05$, ** indicates $p < 0.01$, *** indicates $p < 0.001$.

Full-size DOI: 10.7717/peerj.20476/fig-8

exerts contrary effects under various conditions. During EMT, Matrix Metallopeptidase 13 (MMP13), a key regulator of chondrocyte senescence in Osteoarthritis (OA) (*Zhang et al., 2019b*), is upregulated, contributing to PC metastasis (*Rath et al., 2017*; *Wei et al., 2017*). However, its role in PC cell senescence remains unclear. According to reports, hyperglycemia might promote endothelial senescence *via* the AQR/PLAU axis (*Wan et al., 2022*). Senescent cancer-associated fibroblasts (CAFs) secrete plasminogen activator urokinase (PLAU), driving PC progression and immunosuppression (*Liu et al., 2025*). Additionally, PLAU induces neuronal senescence (*Sun et al., 2024*), highlighting its dual role as an outcome and inducer of SASP. Although senescent Endometrial Mesenchymal Stromal Cell (EMSC)-secreted Insulin-like Growth Factor-Binding Protein 3 (IGFBP3) (*Ushakov et al., 2021*) could induce senescence *via* telomerase inhibition, thus suppressing BC proliferation (*Kwon et al., 2023*), its role in PC senescence remains unclear. On the other hand, Epiregulin (EREG), a senescent stromal cell-secreted soluble factor, was identified as a potential therapeutic target for SASP and could be leveraged to overcome treatment resistance (*Wang et al., 2022a*; *Wang et al., 2022b*). While EREG upregulation in PC tissues could stimulate tumor growth, its silencing inactivates ERK/p38 MAPK pathways, thus inhibiting PDAC (*Liu et al., 2024*; *Zhu et al., 2000*). Nonetheless, the relationship between EREG and PC senescence remains undefined. Regarding DKK1, its knockout in adipose-derived stem cells was reported to activate Wnt signaling, enhancing cell viability, reducing senescence, and suppressing NF-κB-mediated inflammation (*Choi et al., 2024*). Exogenous DKK1 partially rescued FEZ1 inhibition-induced growth arrest and senescence in limbal stem/progenitor cells (*Zhu et al., 2023*). Furthermore, YAP prevented dermal fibroblast senescence and inhibited melanogenesis *via* DKK1 paracrine signaling (*Li et al., 2024*). Additionally, ZEB1 activated the DKK1/mutant p53/Mdm2/CtBP axis and suppressed macroH2A1-mediated senescence, promoting tumorigenesis (*De Barrios et al., 2017*). Finally, ANGPTL4, a key mediator of senescence in diabetic cardiomyopathy, exhibits dual roles. Centrosome amplification-induced SASP promoted tumorigenesis *via* ANGPTL4 secretion (*Wen et al., 2024*). Furthermore, ANGPTL4 accelerated KRAS(G12D)-driven acinar-to-ductal metaplasia and PC initiation (*Yan et al., 2021*). Its overexpression also induced pro-invasive, proliferative, and anti-apoptotic transcriptional programs, conferring gemcitabine resistance and shortening survival in PC (*Gordon et al., 2023*). Herein, bioinformatics analyses revealed ANGPTL4 expression in epithelial, EMT-like, and perivascular cells, correlating with PC prognosis. Functional experiments further demonstrated that recombinant ANGPTL4 could promote PC cell proliferation, invasion, and migration, although its link to senescence remains unclear, necessitating further investigation.

Herein, high-risk patients exhibited reduced naive B cell, memory B cell, plasma cell, and CD8+ T cell infiltration. While B cells amplify anti-tumor immunity *via* antibody production, the presence of plasma cells has been associated with favorable immunotherapy responses (*Delvecchio et al., 2022*; *Mirlekar et al., 2022*). Additionally, IL-35/STAT3/PAX5/BCL6 signaling-driven transcriptional dysregulation in naïve B cells could impair their differentiation into anti-tumor effector cells (*Mirlekar et al., 2022*). *Fan et al. (2024)* reported that DKK1+ tumor cells suppressed CCL19+ fibroblasts and plasma

cell infiltration, contributing to immunotherapy resistance in hepatocellular carcinoma (HCC). Elevated DKK1 levels and reduced plasma cell infiltration in high-risk PC patients suggest similar interactions, warranting further validation. Furthermore, PC patients often exhibit suppressed CD8+ T cell infiltration, which is critical for tumor control. Although MEK/CDK4/6 inhibition-induced SASP enhanced CD8+ T cell infiltration and PD-1 inhibitor sensitivity in PDAC models (*Ruscetti et al., 2020*), our findings of CD8+ T cell downregulation in high-risk patients suggest context-dependent mechanisms. Therefore, given the higher KRAS mutation rates in high-risk patients, combining KRAS pathway inhibitors with PD-1 blockade may enhance CD8+ T cell infiltration, improving outcomes. Primary human senescent CD8+ T cells also exhibit a SASP comprising chemokines, cytokines, and ECM remodeling enzymes (*Callender et al., 2018*). Furthermore, aging cells could express immune surveillance inhibitors and release ligands for the NKG2D receptor, suppressing their clearance, thus weakening the surveillance of aging cells by NK and cytotoxic CD8+ T cells (*Salminen, 2021*). In an age-related inflammation model, cells highly expressing PD-L1 were associated with higher levels of SASP, suggesting that senescent cells specifically express PD-L1 to evade monitoring by CD8+ T cells (*Wang et al., 2022a*; *Wang et al., 2022b*). Moreover, combinations of KRAS inhibitors could induce RB protein-mediated senescence, inhibiting PDAC proliferation. This senescence-inducing therapy triggers SASP, including pro-angiogenic factors that promote tumor angiogenesis. It is also noteworthy that SASP-mediated Endothelial Cell (EC) activation could stimulate CD8+ T cells to aggregate toward immunologically "cold" tumors, making them sensitive to PD-1 checkpoint blockade (*Ruscetti et al., 2020*). Consequently, SASP and immune cells might correlate closely. Overall, age-related diseases may evade surveillance by CD8 T cells and others *via* SASP, while immunotherapy targeting tumors may leverage SASP to reshape the immune IME and achieve antitumor therapeutic effects.

Despite its valuable insights, this study has some limitations. First, we mainly derived SASP genes from published literature, potentially omitting uncharacterized genes. Second, the mechanism linking the seven marker genes in PC with SASP should be verified further in experimental studies. Third, our prognostic model was constructed and validated based solely on public databases. To further validate the reliability of our prognostic signature, additional multicenter clinical cohort studies will be required in the future.

CONCLUSIONS

Herein, we developed a novel SASP-associated molecular subtype and prognostic signature, which may aid in predicting PC prognosis, potentially illuminating PC stratification and therapeutic strategies. Although high-risk patients identified with the model might benefit from combined KRAS pathway inhibition and immunotherapy, further rigorous experimental studies will be required to validate this phenomenon.

ACKNOWLEDGEMENTS

All authors are grateful to the investigators who made their sequencing data publicly available in the ICGC and TCGA databases. We used ChatGPT to assist us in embellishing the English language expressions.

ADDITIONAL INFORMATION AND DECLARATIONS

Funding

The authors received no funding for this work.

Competing Interests

The authors declare there are no competing interests.

Author Contributions

- Yuewen Kuang conceived and designed the experiments, performed the experiments, analyzed the data, prepared figures and/or tables, authored or reviewed drafts of the article, and approved the final draft.
- Mingkun Jia performed the experiments, prepared figures and/or tables, and approved the final draft.
- Yuming Zhu analyzed the data, authored or reviewed drafts of the article, and approved the final draft.
- Zhiyong Xiang conceived and designed the experiments, authored or reviewed drafts of the article, and approved the final draft.

Data Availability

The following information was supplied regarding data availability:

The raw data and code is available in the Supplemental Files.

The data is available at FigShare:

Xiang, Zhiyong; Kuang, Yuewen; Jia, Mingkun; Zhu, Yuming (2025). Analysis of Molecular Subtypes and Prognostic Signature of Senescence-Associated Secretory Phenotype in Pancreatic Cancer. figshare. Dataset. Available at https://doi.org/10.6084/m9.figshare.30621227.v1.

Supplemental Information

Supplemental information for this article can be found online at http://dx.doi.org/10.7717/peerj.20476#supplemental-information.

REFERENCES

Callender LA, Carroll EC, Beal RWJ, Chambers ES, Nourshargh S, Akbar AN, Henson SM. 2018. Human CD8+ EMRA T cells display a senescence-associated secretory phenotype regulated by p38 MAPK. *Aging Cell* **17(1)**:e12675 DOI 10.1111/acel.12675.

Choi N, Hwang J, Kim DY, Kim J, Song SY, Sung J-H. 2024. Involvement of DKK1 secreted from adipose-derived stem cells in alopecia areata. *Cell Proliferation* **57**:e13562 DOI 10.1111/cpr.13562.

De Barrios O, Győrffy B, Fernández-Aceñero MJ, Sánchez-Tilló E, Sánchez-Moral L, Siles L, Esteve-Arenys A, Roué G, Casal JI, Darling DS, Castells A, Postigo A. 2017. ZEB1-induced tumourigenesis requires senescence inhibition *via* activation of DKK1/mutant p53/Mdm2/CtBP and repression of macroH2A1. *Gut* **66**:666–682 DOI 10.1136/gutjnl-2015-310838.

Delvecchio FR, Goulart MR, Fincham REA, Bombadieri M, Kocher HM. 2022. B cells in pancreatic cancer stroma. *World Journal of Gastroenterology* **28**:1088–1101 DOI 10.3748/wjg.v28.i11.1088.

Dong Z, Luo Y, Yuan Z, Tian Y, Jin T, Xu F. 2024. Cellular senescence and SASP in tumor progression and therapeutic opportunities. *Molecular Cancer* **23**:181 DOI 10.1186/s12943-024-02096-7.

Eggert T, Wolter K, Ji J, Ma C, Yevsa T, Klotz S, Medina-Echeverz J, Longerich T, Forgues M, Reisinger F, Heikenwalder M, Wang XW, Zender L, Greten TF. 2016. Distinct functions of senescence-associated immune responses in liver tumor surveillance and tumor progression. *Cancer Cell* **30**:533–547 DOI 10.1016/j.ccell.2016.09.003.

Fan G, Gao R, Xie T, Li L, Tang L, Han X, Shi Y. 2024. DKK1+ tumor cells inhibited the infiltration of CCL19+ fibroblasts and plasma cells contributing to worse immunotherapy response in hepatocellular carcinoma. *Cell Death & Disease* **15**:797 DOI 10.1038/s41419-024-07195-3.

Fleury H, Malaquin N, Tu V, Gilbert S, Martinez A, Olivier MA, Sauriol SA, Communal L, Leclerc-Desaulniers K, Carmona E, Provencher D, Mes-Masson AM, Rodier F. 2019. Exploiting interconnected synthetic lethal interactions between PARP inhibition and cancer cell reversible senescence. *Nature Communications* **10(1)**:2556 DOI 10.1038/s41467-019-10460-1.

González-Gualda E, Pàez-Ribes M, Lozano-Torres B, Macias 3rd D, Wilson JR, González-López C, Ou HL, Mirón-Barroso S, Zhang Z, Lérida-Viso A, Blandez JF, Bernardos A, Sancenón F, Rovira M, Fruk L, Martins CP, Serrano M, Doherty GJ, Martínez-Máñez R, Muñoz Espín D. 2020. Galacto-conjugation of Navitoclax as an efficient strategy to increase senolytic specificity and reduce platelet toxicity. *Aging Cell* **19(4)**:e13142 DOI 10.1111/acel.13142.

Gordon ER, Wright CA, James M, Cooper SJ. 2023. Transcriptomic and functional analysis of ANGPTL4 overexpression in pancreatic cancer nominates targets that reverse chemoresistance. *BMC Cancer* **23**:524 DOI 10.1186/s12885-023-11010-1.

Jia HJ, Rui Bai S, Xia J, Yue He S, Dai QL, Zhou M, Wang XB. 2023. Artesunate ameliorates irinotecan-induced intestinal injury by suppressing cellular senescence and significantly enhances anti-tumor activity. *International Immunopharmacology* **119**:110205 DOI 10.1016/j.intimp.2023.110205.

Klein AP. 2021. Pancreatic cancer epidemiology: understanding the role of lifestyle and inherited risk factors. *Nature Reviews Gastroenterology & Hepatology* **18**:493–502 DOI 10.1038/s41575-021-00457-x.

Kwon A, Chae HW, Lee WJ, Kim J, Kim YJ, Ahn J, Oh Y, Kim H-S. 2023. Insulin-like growth factor binding protein-3 induces senescence by inhibiting telomerase activity in MCF-7 breast cancer cells. *Scientific Reports* **13**:8739 DOI 10.1038/s41598-023-35291-5.

Li T, Xiong Y, Xian L, Xiong L, Li L. 2024. YAP prevents senescence of dermal fibroblast and inhibits melanogenesis *via* paracrine effect of DKK1. *Experimental Dermatology* **33**:e15093 DOI 10.1111/exd.15093.

Liu D, Hornsby PJ. 2007. Senescent human fibroblasts increase the early growth of xenograft tumors *via* matrix metalloproteinase secretion. *Cancer Research* **67**:3117–3126 DOI 10.1158/0008-5472.CAN-06-3452.

Liu L, Huang H, Cheng B, Xie H, Peng W, Cui H, Liang J, Cao M, Yang Y, Chen W, Wang R, Zhao Y. 2025. Revealing the role of cancer-associated fibroblast senescence in prognosis and immune landscape in pancreatic cancer. *iScience* **28**:111612 DOI 10.1016/j.isci.2024.111612.

Liu F, Wu W, Cao W, Feng L, Yuan J, Ren Z, Dai N, Wang X, Li X, Yue S. 2024. EREG silencing inhibits tumorigenesis *via* inactivating ERK/p38 MAPK pathway in pancreatic ductal adenocarcinoma. *Biochimica et Biophysica Acta: Molecular Basis of Disease* **1870**:167336 DOI 10.1016/j.bbadis.2024.167336.

McHugh D, Durán I, Gil J. 2025. Senescence as a therapeutic target in cancer and age-related diseases. *Nature Reviews Drug Discovery* **24**:57–71 DOI 10.1038/s41573-024-01074-4.

Milanovic M, Fan DNY, Belenki D, Däbritz JHM, Zhao Z, Yu Y, Dörr JR, Dimitrova L, Lenze D, Monteiro Barbosa IA, Mendoza-Parra MA, Kanashova T, Metzner M, Pardon K, Reimann M, Trumpp A, Dörken B, Zuber J, Gronemeyer H, Hummel M, Dittmar G, Lee S, Schmitt CA. 2018. Senescence-associated reprogramming promotes cancer stemness. *Nature* **553**(**7686**):96–100 DOI 10.1038/nature25167.

Mirlekar B, Wang Y, Li S, Zhou M, Entwistle S, De Buysscher T, Morrison A, Herrera G, Harris C, Vincent BG, Ting JP-Y, Rashid N, Kim WY, Yeh JJ, Pylayeva-Gupta Y. 2022. Balance between immunoregulatory B cells and plasma cells drives pancreatic tumor immunity. *Cell Reports Medicine* **3**:100744 DOI 10.1016/j.xcrm.2022.100744.

Mizrahi JD, Surana R, Valle JW, Shroff RT. 2020. Pancreatic cancer. *The Lancet* **395**:2008–2020 DOI 10.1016/S0140-6736(20)30974-0.

Nacarelli T, Lau L, Fukumoto T, Zundell J, Fatkhutdinov N, Wu S, Aird KM, Iwasaki O, Kossenkov AV, Schultz D, Noma K-I, Baur JA, Schug Z, Tang H-Y, Speicher DW, David G, Zhang R. 2019. NAD+ metabolism governs the proinflammatory senescence-associated secretome. *Nature Cell Biology* **21**:397–407 DOI 10.1038/s41556-019-0287-4.

Nardella C, Clohessy JG, Alimonti A, Pandolfi PP. 2011. Pro-senescence therapy for cancer treatment. *Nature Reviews Cancer* **11**(**7**):503–511 DOI 10.1038/nrc3057.

Nevala-Plagemann C, Hidalgo M, Garrido-Laguna I. 2020. From state-of-the-art treatments to novel therapies for advanced-stage pancreatic cancer. *Nature Reviews Clinical Oncology* **17**:108–123 DOI 10.1038/s41571-019-0281-6.

Ohuchida K, Mizumoto K, Murakami M, Qian L-W, Sato N, Nagai E, Matsumoto K, Nakamura T, Tanaka M. 2004. Radiation to stromal fibroblasts increases invasiveness of pancreatic cancer cells through tumor-stromal interactions. *Cancer Research* **64**:3215–3222 DOI 10.1158/0008-5472.can-03-2464.

Orjalo AV, Bhaumik D, Gengler BK, Scott GK, Campisi J. 2009. Cell surface-bound IL-1alpha is an upstream regulator of the senescence-associated IL-6/IL-8 cytokine network. *Proceedings of the National Academy of Sciences of the United States of America* **106**:17031–17036 DOI 10.1073/pnas.0905299106.

Park W, Chawla A, O'Reilly EM. 2021. Pancreatic cancer: a review. *JAMA* **326**:851–862 DOI 10.1001/jama.2021.13027.

Purcell M, Kruger A, Tainsky MA. 2014. Gene expression profiling of replicative and induced senescence. *Cell Cycle* **13(24)**:3927–3937 DOI 10.4161/15384101.2014.973327.

Rahib L, Wehner MR, Matrisian LM, Nead KT. 2021. Estimated projection of us cancer incidence and death to 2040. *JAMA Network Open* **4**:e214708 DOI 10.1001/jamanetworkopen.2021.4708.

Rath N, Morton JP, Julian L, Helbig L, Kadir S, McGhee EJ, Anderson KI, Kalna G, Mullin M, Pinho AV, Rooman I, Samuel MS, Olson MF. 2017. ROCK signaling promotes collagen remodeling to facilitate invasive pancreatic ductal adenocarcinoma tumor cell growth. *EMBO Molecular Medicine* **9**:198–218 DOI 10.15252/emmm.201606743.

Ruscetti M, Morris JP, Mezzadra R, Russell J, Leibold J, Romesser PB, Simon J, Kulick A, Ho Y-J, Fennell M, Li J, Norgard RJ, Wilkinson JE, Alonso-Curbelo D, Sridharan R, Heller DA, De Stanchina E, Stanger BZ, Sherr CJ, Lowe SW. 2020. Senescence-induced vascular remodeling creates therapeutic vulnerabilities in pancreas cancer. *Cell* **181**:424–441.e21 DOI 10.1016/j.cell.2020.03.008.

Salminen A. 2021. Feed-forward regulation between cellular senescence and immunosuppression promotes the aging process and age-related diseases. *Ageing Research Reviews* **67**:101280 DOI 10.1016/j.arr.2021.101280.

Saul D, Kosinsky RL, Atkinson EJ, Doolittle ML, Zhang X, LeBrasseur NK, Pignolo RJ, Robbins PD, Niedernhofer LJ, Ikeno Y, Jurk D, Passos JF, Hickson LJ, Xue A, Monroe DG, Tchkonia T, Kirkland JL, Farr JN, Khosla S. 2022. A new gene set identifies senescent cells and predicts senescence-associated pathways across tissues. *Nature Communications* **13**:4827 DOI 10.1038/s41467-022-32552-1.

Schilbach K, Welker C, Krickeberg N, Kaißer C, Schleicher S, Hashimoto H. 2020. In the absence of a TCR signal IL-2/IL-12/18-stimulated $\gamma\delta$ T cells demonstrate potent anti-tumoral function through direct killing and senescence induction in cancer cells. *Cancers* **12**:130 DOI 10.3390/cancers12010130.

Sharma M, Hunter KD, Fonseca FP, Radhakrishnan R. 2021. Emerging role of cellular senescence in the pathogenesis of oral submucous fibrosis and its malignant transformation. *Head & Neck* **43**:3153–3164 DOI 10.1002/hed.26805.

Siegel RL, Miller KD, Wagle NS, Jemal A. 2023. Cancer statistics, 2023. *CA: A Cancer Journal for Clinicians* **73**:17–48 DOI 10.3322/caac.21763.

Sun W, Sheng X, Li P, Li R, Guo Z, Lin H, Gong Y. 2024. Identification of vilazodone as a novel plasminogen activator inhibitor to overcome Alzheimer's disease through virtual screening, molecular dynamics simulation, and biological evaluation. *Archiv der Pharmazie* **357**:e2400263 DOI 10.1002/ardp.202400263.

Thul PJ, Åkesson L, Wiking M, Mahdessian D, Geladaki A, Ait Blal H, Alm T, Asplund A, Björk L, Breckels LM, Bäckström A, Danielsson F, Fagerberg L, Fall J, Gatto L, Gnann C, Hober S, Hjelmare M, Johansson F, Lee S, Lindskog C, Mulder J, Mulvey CM, Nilsson P, Oksvold P, Rockberg J, Schutten R, Schwenk JM, Sivertsson Å, Sjöstedt E, Skogs M, Stadler C, Sullivan DP, Tegel H, Winsnes C, Zhang C, Zwahlen M, Mardinoglu A, Pontén F, von Feilitzen K, Lilley KS, Uhlén M, Lundberg E. 2017. A subcellular map of the human proteome. *Science* **356**:eaal3321 DOI 10.1126/science.aal3321.

Ushakov RE, Aksenov ND, Pugovkina NA, Burova EB. 2021. Effects of IGFBP3 knockdown on human endometrial mesenchymal stromal cells stress-induced senescence. *Biochemical and Biophysical Research Communications* **570**:143–147 DOI 10.1016/j.bbrc.2021.07.046.

Wan Y, Liu Z, Wu A, Khan AH, Zhu Y, Ding S, Li X, Zhao Y, Dai X, Zhou J, Liu J, Li Y, Gong X, Liu M, Tian X-L. 2022. Hyperglycemia promotes endothelial cell senescence through AQR/PLAU signaling axis. *International Journal of Molecular Sciences* **23**:2879 DOI 10.3390/ijms23052879.

Wang B, Han J, Elisseeff JH, Demaria M. 2024. The senescence-associated secretory phenotype and its physiological and pathological implications. *Nature Reviews Molecular Cell Biology* **25**:958–978 DOI 10.1038/s41580-024-00727-x.

Wang TW, Johmura Y, Suzuki N, Omori S, Migita T, Yamaguchi K, Hatakeyama S, Yamazaki S, Shimizu E, Imoto S, Furukawa Y, Yoshimura A, Nakanishi M. 2022b. Blocking PD-L1-PD-1 improves senescence surveillance and ageing phenotypes. *Nature* **611(7935)**:358–364 DOI 10.1038/s41586-022-05388-4.

Wang C, Long Q, Fu Q, Xu Q, Fu D, Li Y, Gao L, Guo J, Zhang X, Lam EW-F, Campisi J, Sun Y. 2022a. Targeting epiregulin in the treatment-damaged tumor microenvironment restrains therapeutic resistance. *Oncogene* **41**:4941–4959 DOI 10.1038/s41388-022-02476-7.

Wang X, Zhang C, Yan X, Lan B, Wang J, Wei C, Cao X, Wang R, Yao J, Zhou T, Zhou M, Liu Q, Jiang B, Jiang P, Kesari S, Lin X, Guo F. 2016. A novel bioavailable BH3 mimetic efficiently inhibits colon cancer *via* cascade effects of mitochondria. *Clinical Cancer Research* **22(6)**:1445–1458 DOI 10.1158/1078-0432.CCR-15-0732.

Wei H, Xu Z, Liu F, Wang F, Wang X, Sun X, Li J. 2017. Hypoxia induces oncogene yes-associated protein 1 nuclear translocation to promote pancreatic ductal adenocarcinoma invasion *via* epithelial-mesenchymal transition. *International Society for Oncodevelopmental Biology and Medicine* **39**:1010428317691684 DOI 10.1177/1010428317691684.

Wen Y, Zhang X, Liu H, Ye H, Wang R, Ma C, Duo T, Wang J, Yang X, Yu M, Wang Y, Wu L, Zhao Y, Wang L. 2024. SGLT2 inhibitor downregulates ANGPTL4 to mitigate pathological aging of cardiomyocytes induced by type 2 diabetes. *Cardiovascular Diabetology* **23**:430 DOI 10.1186/s12933-024-02520-8.

Wu SK, Ariffin J, Tay SC, Picone R. 2023. The variant senescence-associated secretory phenotype induced by centrosome amplification constitutes a pathway that activates hypoxia-inducible factor-1α. *Aging Cell* **22**:e13766 DOI 10.1111/acel.13766.

Xiao S, Qin D, Hou X, Tian L, Yu Y, Zhang R, Lyu H, Guo D, Chen XZ, Zhou C, Tang J. 2023. Cellular senescence: a double-edged sword in cancer therapy. *Frontiers in Oncology* **13**:1189015 DOI 10.3389/fonc.2023.1189015.

Yan HH, Jung KH, Lee JE, Son MK, Fang Z, Park JH, Kim SJ, Kim JY, Lim JH, Hong S-S. 2021. ANGPTL4 accelerates KRASG12D-Induced acinar to ductal metaplasia and pancreatic carcinogenesis. *Cancer Letters* **519**:185–198 DOI 10.1016/j.canlet.2021.07.036.

Yang L, Xing S, Wang K, Yi H, Du B. 2018. Paeonol attenuates aging MRC-5 cells and inhibits epithelial-mesenchymal transition of premalignant HaCaT cells induced by aging MRC-5 cell-conditioned medium. *Molecular and Cellular Biochemistry* **439**:117–129 DOI 10.1007/s11010-017-3141-7.

Zhang H-R, Li T-J, Yu X-J, Liu C, Wu W-D, Ye L-Y, Jin K-Z. 2024. The GFPT2-O-GlcNAcylation-YBX1 axis promotes IL-18 secretion to regulate the tumor immune microenvironment in pancreatic cancer. *Cell Death & Disease* **15**:244 DOI 10.1038/s41419-024-06589-7.

Zhang W, Zhang C, Luo C, Zhan Y, Zhong B. 2019b. Design, cyclization, and optimization of MMP13-TIMP1 interaction-derived self-inhibitory peptides against chondrocyte senescence in osteoarthritis. *International Journal of Biological Macromolecules* **121**:921–929 DOI 10.1016/j.ijbiomac.2018.10.141.

Zhang L-M, Zhang J, Zhang Y, Fei C, Wang L, Yi Z-W, Zhang Z-Q. 2019a. Interleukin-18 promotes fibroblast senescence in pulmonary fibrosis through down-regulating Klotho expression. *Biomedicine & Pharmacotherapy* **113**:108756 DOI 10.1016/j.biopha.2019.108756.

Zhu Z, Kleeff J, Friess H, Wang L, Zimmermann A, Yarden Y, Büchler MW, Korc M. 2000. Epiregulin is Up-regulated in pancreatic cancer and stimulates pancreatic cancer cell growth. *Biochemical and Biophysical Research Communications* **273**:1019–1024 DOI 10.1006/bbrc.2000.3033.

Zhu L, Wang L, Liu D, Chen C, Mo K, Lan X, Liu J, Huang Y, Guo D, Huang H, Li M, Guo H, Tan J, Zhang K, Ji J, Yuan J, Ouyang H. 2023. Single-cell transcriptomics implicates the FEZ1-DKK1 axis in the regulation of corneal epithelial cell proliferation and senescence. *Cell Proliferation* **56**:e13433 DOI 10.1111/cpr.13433.